Self-assembled Monolayer Mediated Surface Environment Modification of Poly(vinylpyrrolidone)-Coated Hollow Au−Ag Nanoshells for Enhanced Loading of Hydrophobic Drug and Efficient Multimodal Therapy

Hongje Jang,[†] Dong-Eun Kim,[‡] and Dal-Hee Min*[†,§]

[†]Department of Chemistry, Center for RNA Research, Institute for Basic Sciences (IBS), Seoul National University, Seoul 151-747, Republic of Korea
[‡]Department of Bioscience and Biotechnology, Konkuk University, Seoul 143-701, Republic of Korea
[§]Lemonex Inc., Seoul 151-742, Republic of Korea

S *Supporting Information*

ABSTRACT: Hollow Au−Ag bimetallic nanoshell possessing hydrophobic interior space and hydrophilic exterior surface was prepared and its application as a chemo-thermo-gene therapeutic agent based on its high payload of multiple drugs having different water solubility was demonstrated. The multifunctional drug delivery system is based on the hydrophobic interior created by the self-assembled monolayer (SAM) of hexanethiol onto the inner surface of the hollow metallic nanoshells whereas the outer surface was mostly coated by hydrophilic biocompatible polymer. The nanoshells having surface environment modified by hexanethiol SAMs provided high capacity both for hydrophilic DNAzyme (Dz) to induce gene silencing and for hydrophobic SN38 (7-ethyl-10-hydroxycampto-thecin), anticancer drug. The release of the loaded Dz and SN38 was independently triggered by an acidic environment and by photothermal temperature elevation upon irradiation, respectively. The chemo-thermo-gene multitherapy based on the present nanoshells having modified surface environment showed high efficacy in quantitative cell-based assays using Huh7 human liver cell containing hepatitis C viral NS3 gene replicon RNA.

KEYWORDS: *chemotherapy, drug delivery, hollow nanoshells, photothermal therapy, self-assembled monolayer*
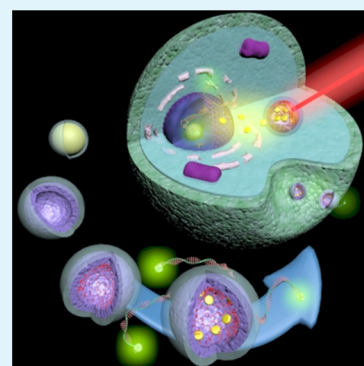
INTRODUCTION

Hollow gold nanoshells have been studied for decades due to the unique physicochemical properties including controllable diameter and shell thickness,[1−3] hollow structure useful for cargo loading,[4,5] high surface-to-volume ratio and distinctive surface plasmon resonance (SPR).[6,7] Among them, photo-thermal conversion effect, in which absorption around near-infrared (NIR) wavelength region induces the conversion of absorbed light into heat, was observed in the plasmonic Au nanostructures, and has been employed for cancer treat-ment,[8−12] stimuli-induced drug release,[13,14] and photothermal interference contrast imaging.[15] Moreover, the wavelength superposition between SPR and optical window[16,17] in body fluids and tissue chromophores including hemoglobin makes gold nanoshells absorbing NIR light compatible with in vivo photothermal applications.[18] The remarkable set of optical and physical properties has made hollow gold nanoshells one of the most promising nanostructures for diverse biomedical applications.

Self-assembled monolayers (SAM) are molecular assemblies of organic molecules on surfaces formed by spontaneous adsorption of molecules. SAM provides a convenient and effective way of modulating the surface environment as desired, such as introducing specific functional groups on a target surface with control over density and fine-tuning hydrophilicity or hydrophobicity of a solid substrate surface. These advantages of SAM in controlling surface chemistry of substrate with simple, highly versatile, and inexpensive manner encouraged the development of diverse analytical and biomedical applications of gold nanostructures including catalysis,[19−21] patterning,[22−24] drug screening,[25,26] biosensors,[27−29] and drug delivery platforms.[30−32]

Here, we synthesized poly(vinylpyrrolidone) (PVP)-coated hollow Au−Ag alloy nanoshells (PVP-HANs) through galvanic replacement reaction of sacrificial PVP-coated Ag nanoparticles (PVP-AgNPs). Galvanic replacement is spontaneous replace-ment reaction driven by standard reduction potential difference between two elements. Because of the advantages of simplicity and ease of preparation of homogeneous and highly crystalline structure without cytotoxic surfactants, galvanic replacement is
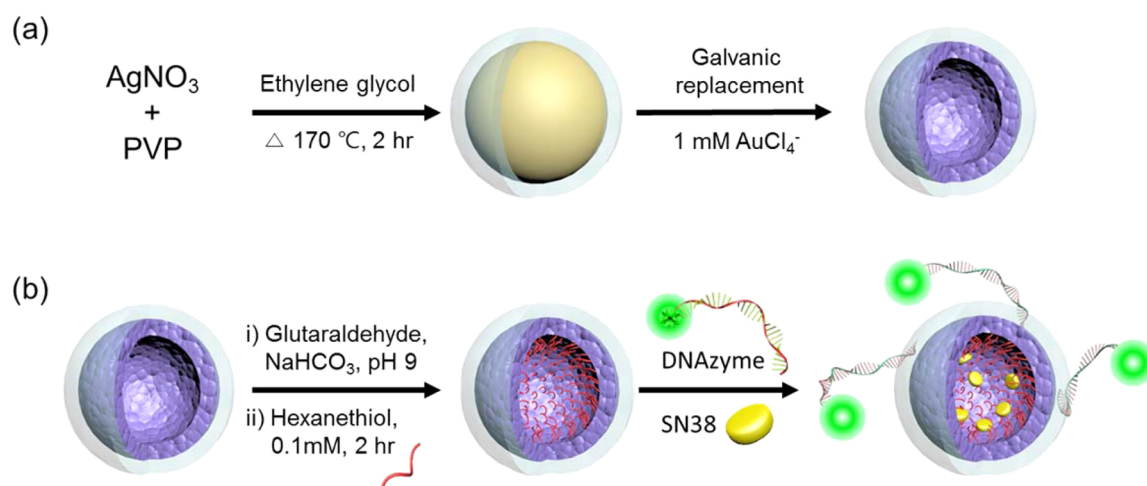
Figure 1. Scheme of SN38/Dz-loaded PVP-HAN preparation. (a) PVP-HANs were prepared by galvanic replacement reaction of as-synthesized PVP-AgNPs under ambient condition. (b) Aldehyde functional group was introduced on the outer surface of the prepared PVP-HAN, followed by generation of hydrophobic interior via formation of SAM. Dye-labeled Dz was conjugated by imine linkage formation and SN38 was loaded through hydrophobic interaction.

widely used in preparation of various nanostructures not only hollow but also clustered particles.[33] The prepared PVP-HANs exhibited excellent colloidal stability in aqueous solvent due to the exterior PVP surface coating which is hydrophilic and biocompatible FDA-approved polymer. Next, we generated hydrophobic interior surface onto the hollow Au−Ag nanoshells by hydrophobic alkanethiol SAM formation dominantly onto the inner surface of the cavity because the PVP coating is present mostly on the outer surface of nanoshells. The prepared amphiphilic Au−Ag nanoshell having hydrophobic interior and hydrophilic exterior was employed to load small molecule drugs insoluble in aqueous solvent via hydrophobic interactions with interior surface inside the cavity of the nanoshells, and to load hydrophilic oligonucleotides to induce knockdown of target gene responsible for disease with sequence specificity onto the exterior surface of nanoshells via Schiff base formation. The present multidrug nanocomplex provided a unique feature of independently controllable drug release capability in which the release of hydrophobic drugs were controlled by photothermal conversion upon NIR irradiation whereas the release of oligonucleotide was triggered by pH change from 7.4 to 5.0. If applicable, hyperthermia itself can be utilized as another modality as therapeutics to eradicate target cells in addition to small-molecule drug and oligonucleotide. We demonstrated that highly efficient cellular delivery of the multidrug nanocomplex entailing NIR irradiation induced almost complete cell death by synergistic chemo-thermo multitherapy. To the best of our knowledge, it is the first to prepare the nanoshells possessing a highly hydrophobic interior generated by SAM formation as well as a hydrophilic biocompatible exterior surface and to employ for loading two different types of drugs with very high payload, providing independently controllable drug release capability.

Hepatitis C is a serious disease caused by hepatitis C virus (HCV) infection, which is one major cause of chronic liver damage such as liver cirrhosis and hepatocellular carcinoma. Current standard treatment for hepatitis C is combination therapy involving interferon-α and ribavirin, which shows numerous side effects including birth defects and depression.[34] Although drug candidates to block HCV replication were recently developed, new efficient therapeutic options are still

urgently needed. In the present study, to demonstrate our new strategy using amphiphilic nanoshells as multidrug carriers to treat hepatitis C, we adopted extremely hydrophobic 7-ethyl-10-hydroxycamptothecin (SN38),[35] which is insoluble small-molecule drug (metabolite of irinotecan, topoisomerase I inhibitor) in aqueous solvent and hydrophilic 10-23 DNAzyme (deoxyribozyme, Dz, catalytic DNA molecule)[36] to silence NS3 gene region of HCV as drugs to load inside and outside of the amphiphilic Au−Ag nanoshells, respectively. Dz is a single-stranded DNA composed of catalytic core region and sequence-recognizing arm region, exhibiting catalytic activity to cleave target RNA strand and, as a result, to silence target gene by inhibiting translation of mRNA to corresponding protein. The Dz sequence used in the present study is designed to knockdown NS3 gene of HCV which encodes helicase, one of the critical enzymes required for HCV replication. In cell-based assays for the present study, we used Huh7 cells carrying HCV replicon (Luc-Neo NS3 replicon Huh7)[37] where silencing of NS3 gene reduced cell viability in cell media containing an antibiotic, G418 (also called as Geneticin). The delivery strategy of Dz was previously reported many times by using various nanomaterials including gold nanoparticle, iron oxide nanoparticle, graphene oxide, polymers, and lyposome.[38−40] In the case of the delivery of highly hydrophobic SN38, there are fewer reports utilizing graphene oxide, polymer, and mesoporous silica nanoparticle. Since the mechanism of therapeutic effect induced by Dz (oligonucleotide for gene therapy) and SN38 (small-molecule inhibitor of topoisomerase I) is very different from each other, we could expect synergistic therapeutic effect by codelivery of these two different types of drugs. In addition, the present approach could be a good model system to demonstrate codelivery of hydrophilic and hydrophobic drugs by using one nanocarrier.[41−43]

■ RESULTS AND DISCUSSION

First, sacrificial PVP-AgNPs were prepared by a previously reported polyol method with slight modification.[44] Galvanic replacement reaction was then performed with addition of 100 μL of 1 mM AuCl$_4^-$ solution in distilled water to 1 mL of 250 pM as-synthesized PVP-AgNPs to prepare PVP-HANs. The
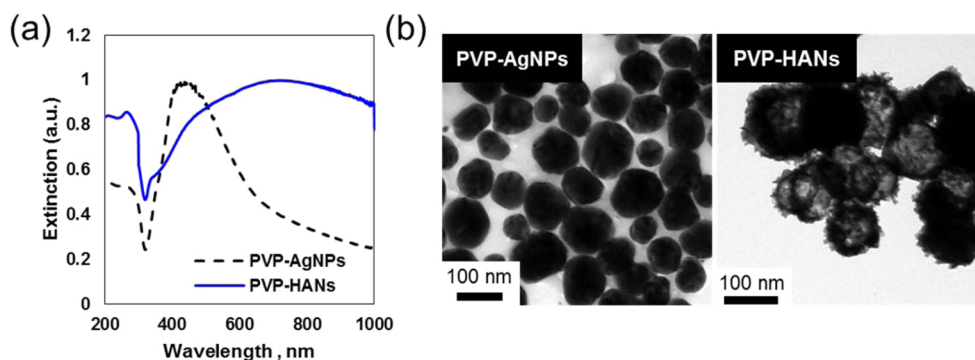
Figure 2. Characterization of the synthesized PVP-AgNPs and PVP-HANs. (a) Red shift of the SPR band in UV−vis absorption spectrum and (b) TEM image showing the formation of hollow structure with 100 nm diameter. Scale bars are 100 nm in all images.

replacement reaction was completed within 10 min at room temperature with stirring, which was confirmed by the change of color and SPR band (Figure 1a). UV−vis spectrophotometry of PVP-AgNPs and the replaced PVP-HANs clearly supported the evidence of hollow nanoshell structure formation by distinctive SPR red shift from 450 to 719 nm (Figure 2a). Transmission electron microscopy (TEM) and high-angle annular dark-field scanning transmission electron microscopy/ energy-dispersive spectrometry (HAADF-STEM/EDS) showed structures and Ag−Au elemental deposition aspect of PVP-AgNPs and PVP-HANs (Figure 2b and Figure S1 of the Supporting Information). According to the EDS line profiling, PVP-AgNPs exhibited maximum Ag counts at the profiling path center with quasi-parabolic distribution without any Au intensity and PVP-HANs represented maximum Au counts from both profiling path ends with reduced Ag distribution. These observations fit perfectly with their nanostructure transformation from spherical into hollow nanoshells accompanied by the elemental replacement of Ag into Au.

Next, for the preparation of amphiphilic hollow Au−Ag nanoshells, hydrophobic alkanethiol SAM was formed on the surface of the prepared PVP-HANs by addition of alkanethiols with different carbon chain lengths (n = 6, 8, 12, and 16) to final concentration of 0.1 mM in 10% ethanol solution, followed by incubation for 2 h at room temperature. Among four different alkanethiols, we found that hexanethiol-treated PVP-HANs (Hex-PVP-HANs) were well-dispersed in distilled water, whereas octane-, dodecane-, and hexadecanethiol-treated nanoshells showed aggregations in distilled water. Therefore, we assume that alkanethiol SAM could be formed onto some portion of the exterior surface in addition to the interior surface, but to a much lesser degree than the interior surface. We think that part of the exterior PVP coating of sacrificial AgNPs could become loose during galvanic replacement reaction, resulting in exposed metal surface available for SAM formation. On the other hand, galvanic replacement reaction makes fully exposed interior surface available for the adsorption of alkanethiols. The formation of hexanethiol SAM was first characterized by SPR shift from 719 to 758 nm in UV−vis spectra (Figure S2a). We observed no structural difference of the nanoshells before and after hexanethiol SAM formation in TEM images (Figure S2b). In the case of hexanethiol ligands, even if the hydrophobic alkanethiol ligands could be adsorbed on the exterior surface, relatively short carbon chain length did not significantly affect the overall hydroaffinity of the external environment because of the thick hydrophilic PVP shells, unlike longer chains (n = 8, 12, and 16) (Figure S3). Therefore, for

the sake of convenience, we describe that the environment of the interior surface is hydrophobic and the exterior surface is hydrophilic after SAM formation of hexanethiol since the exterior surface is still considered as much more hydrophilic compared to the interior surface of the nanoshells.

To assess the formation of the hydrophobic environment on the interior surface, we next performed the loading of SN38, hydrophobic drug, and before and after SAM formation. Because of the poor solubility of SN38 in aqueous solvent, PVP-HANs and Hex-PVP-HANs were first dispersed in dimethyl sulfoxide (DMSO) and mixed with 10 μM of SN38 in DMSO. After the 3 h of incubation at room temperature, unloaded SN38 was removed by centrifugation with sequential solvent exchange to distilled water. We estimated the amount of the loaded SN38 to PVP-HANs and Hex-PVP-HANs from the extinction coefficient of SN38 ($\varepsilon_{SN38,380\ nm}$ = 25 500 mol^{-1} cm^{-1}) and UV−vis absorbance measurement of the SN38-loaded nanoshells.[45] In the case of Hex-PVP-HANs carrying hydrophobic SAM, loading capacity for SN38 (7950 SN38/ Hex-PVP-HAN) was about 30 times higher than nanoshells omitting SAM (260 SN38/PVP-HAN) (Figure 3a,b).
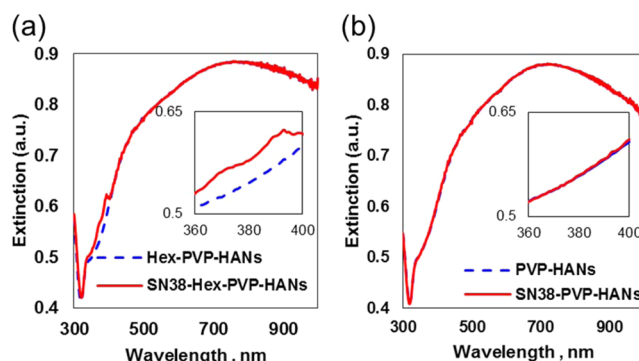

Figure 3. Enhancement of SN38 loading capacity by hydrophobic hexanethiol SAM formation inside the nanoshell was characterized by UV−vis absorption and fluorescence emission spectroscopy. (a) Formation of hydrophobic hexanethiol SAM greatly enhanced the loading capacity of SN38 compared to (b) nanoshells omitting SAMs.

Next, we utilized Schiff base linkage formation to load fluorescein (FAM)-labeled Dz amine (FDz) to the PVP-HANs. To demonstrate the strategy, aldehyde functional group was first introduced by previously reported reaction of surface PVP with glutaraldehyde in pH 9 sodium bicarbonate solution, prior to the hexanethiol SAM formation.[46] FDz was then conjugated
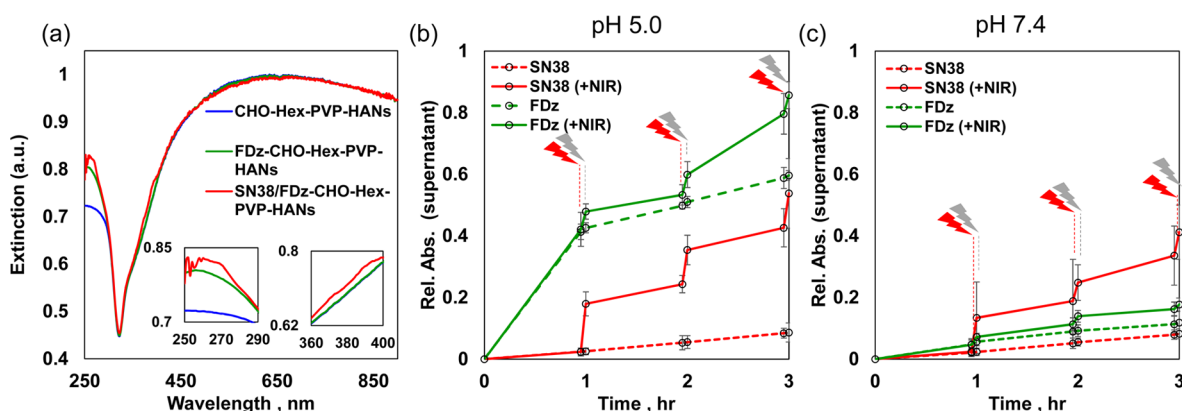
Figure 4. Characterization of loading of SN38/FDz to CHO-Hex-PVP-HANs and release profile of loaded cargos. (a) UV−vis absorption spectra of the nanoshells loaded with SN38/FDz onto interior/exterior surface were obtained and the amount of loaded SN38 and FDz were calculated based on UV−vis absorption. According to estimation using extinction coefficients, 520 FDz molecules and 4030 SN38 molecules were loaded onto CHO-Hex-PVP-HANs. Insets are enlarged plot for loading profiling of FDz (left, from 250 to 290 nm) and SN38 (right, from 360 to 400 nm). (b, c) In the drug release profile, the release of FDz conjugated via imine linkage was expedited in acidic solution (59.6% at pH 5.0 in (b)) than in neutral solution (11.8% at pH 7.4 in (c)) without NIR irradiation after 3 h of incubation. With NIR irradiation, 85.7% and 17.7% of FDz release was observed at pH 5.0 and pH 7.4, respectively. However, the release of SN38 was hardly affected only by pH change. The release of SN38 was mainly affected by repeated NIR irradiation and was slightly favored at acidic pH (8.6% and 8.2% release at pH 5.0 and pH 7.4, respectively, without NIR and 53.8% and 41.2% release at pH 5.0 and pH 7.4, respectively, with NIR.

onto the exterior CHO-PVP hydrophilic coating (CHO denoted rational formula of introduced aldehyde functional groups onto PVP) of hollow gold nanoshells (CHO-Hex-PVP-HANs) through Schiff base imine linkage and SN38 was next loaded into interior hydrophobic hexanethiol SAM surface through diffusion (Figure 1b). The amounts of the loaded SN38 and FDz were calculated as 520 FDz and 4030 SN38 per CHO-Hex-PVP-HAN from UV−vis absorption spectra of the SN38/FDz-loaded nanoshells by using each extinction coefficient of SN38 and FDz (Figure 4a). The SN38 loading capacity of CHO-Hex-PVP-HANs was 50% lower than that of Hex-PVP-HANs, suggesting that probably the increased hydrophilicity and steric hindrance generated by conjugation of FDz on the exterior surface could decrease the loading capacity of SN38. Nonetheless, the payload of SN38 was still 15 times higher in FDz-CHO-Hex-PVP-HANs than in PVP-HANs omitting hydrophobic SAM.

To demonstrate SN38/FDz/NIR chemo-thermo gene multi-therapy, we first investigated photothermal effect of PVP-HAN derivatives along with the irradiation of 808 nm NIR laser. In comparison with the temperature elevation of distilled water (ΔT = 1.8 °C) and PVP-AgNPs (ΔT = 4.2 °C), PVP-HANs derivatives showed much higher temperature elevation (ΔT = 47.2 and 49.4 °C from PVP-HANs and CHO-Hex-PVP-HANs, respectively, with irradiation at 0.4 W/cm^2 for 2 min). This level of temperature elevation is known to be sufficient to induce cell hyperthermia or to release loaded drugs (Figure S4a).[47] Luc-Neo NS3 replicon Huh7 cell line, human liver cell line carrying HCV replicon, was next treated with the CHO-Hex-PVP-HANs, followed by 808 nm NIR laser irradiation (8 W/cm^2, 5 min) at designated area. Live/dead staining showed that selective cell death only in designated region (Figure S4b). Next, to ensure the release of loaded SN38/FDz under specific stimuli, we performed cargo releasing test with or without NIR irradiation in pH 5 and pH 7.4 buffer solution, respectively. The acidic condition of pH 5 was used for mimicking the late endosomal/lysosomal condition after endocytosis. The 0.4 W/cm^2 NIR irradiation was repeated over a period of 3 min, followed by 57 min of intervals for a total of 3 h. We observed

the notably enhanced release of FDz in acidic solution by the breakage of Schiff base imine linkage. The NIR irradiation also induced burst release of SN38 and FDz compared to control group without irradiation which showed steady release (Figure 4b).

Prior to chemo-thermo gene multitherapeutic efficacy assay, we measured the cytotoxicity of CHO-PVP-HANs and CHO-Hex-PVP-HANs toward NS3 replicon Huh7 cells by 3-(4,5-dimethylthiazol-2-yl)-2,5-diphenyl tetrazolium bromide (MTT) cell viability assay and live/dead staining. MTT assay showed that both nanoshells exhibited no notable cytotoxicity up to 50 pM, and showed over 60% of cell viability even at 200 pM. The low cytotoxicity might be originated from several features. First, during the galvanic replacement reaction, easily dissolvable or releasable Ag might already be replaced with Au and remaining Ag compositions are relatively stable. Second, the surface PVP polymer coating is expected to play a protective role to inhibit the dissolution of Ag. Relatively low cytotoxicity of polymer-coated Au−Ag alloy nanoshells was previously reported in which dextran was used as a surface-coating polymer.[33] In the present study, the highest concentration of the CHO-Hex-PVP-HANs used was 50 pM at which over 90% of cell viability was ensured (Figure S5).

We next investigated therapeutic efficacy of the drug/gene nanoshell complex by using 50 pM CHO-Hex-PVP-HANs loaded with 25.8 nM FDz and 201 nM SN38. According to viability assay using NS3 replicon Huh7 cells, dramatic cell viability decreasing down to 1.2% was observed in the experimental set of SN38/FDz-CHO-Hex-PVP-HANs with 808 nm NIR irradiation (1 W/cm^2, 5 min), whereas 11.3% of cell viability was observed with treatment of the same nanoshell complex without irradiation. The used NIR laser power and irradiation time were considered appropriate to observe the clear relationship between chemo and thermo multitherapy. In this experimental condition, isolated NIR irradiation induced little viability decrease to 93.4%. In addition, nanoshells carrying only SN38 (40.3% of viability) or only FDz (30.2%) showed higher therapeutic efficacy than free SN38 (65.2%) and free FDz (95.4%) (Figure 5a). Collectively, the amphiphilic
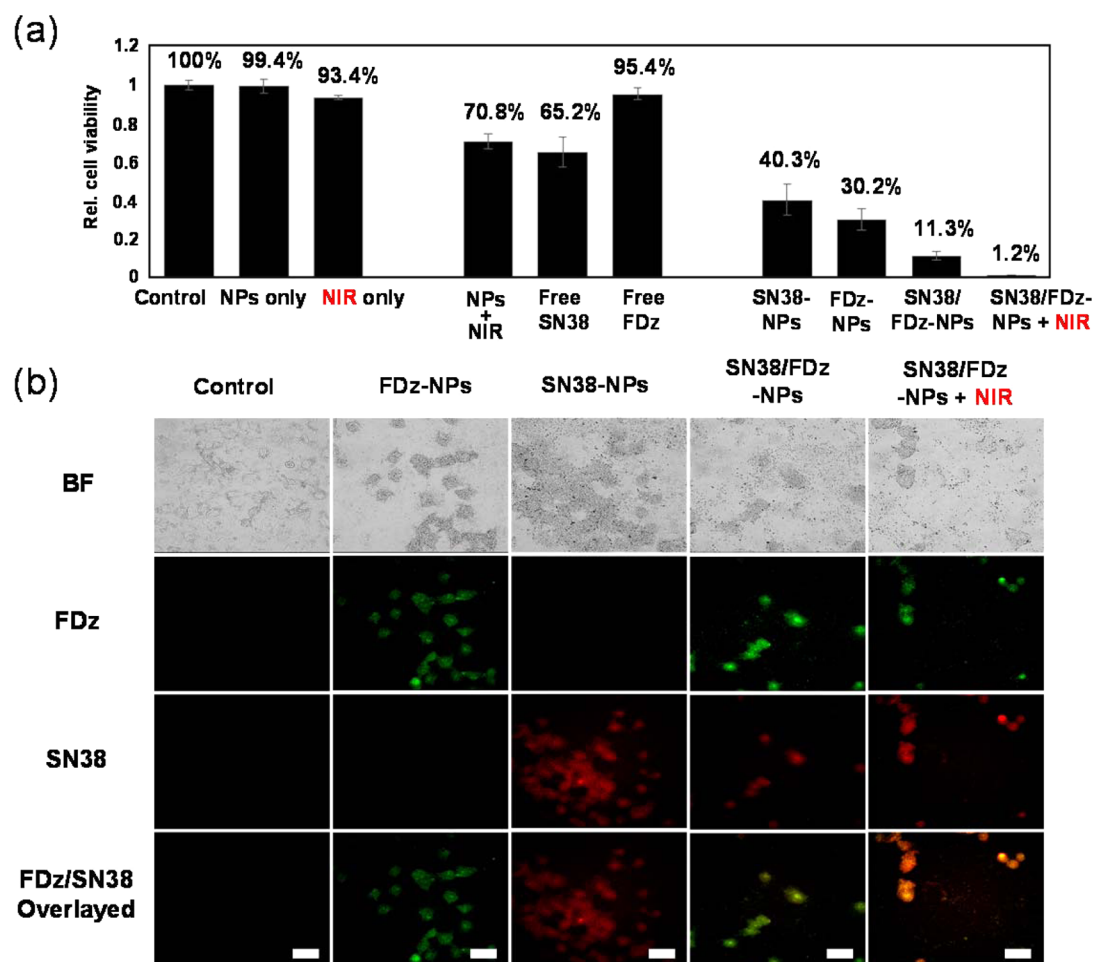
Figure 5. Quantitative viability assay of NS3 replicon Huh7 cells treated with SN38 and/or FDz-loaded CHO-Hex-PVP-HANs. (a) Nanoshells loaded with SN38/FDz reduced cell viability down to 11.3%, and additional NIR irradiation improved therapeutic effect showing cell viability decrease down to 1.2%. Treatment of nanoshells loaded with SN38 alone (viability = 40.3%) or FDz alone (30.2%) exhibited enhanced therapeutic efficacy compared to free SN38 (65.2%) or free FDz (95.4%) treatment. As controls, cells treated with only NIR irradiation or empty nanoshells exhibited negligible decrease of cell viability. (b) Fluorescence images of NS3 replicon Huh7 cells after treatment showed the successful delivery of loaded cargos and NIR-mediated enhanced release of SN38. The scale bar is 50 μm.

PVP-HANs modified with hydrophobic SAM was successfully employed as a convenient nanocarrier to deliver both hydrophilic and hydrophobic cargos separately or simultaneously. From the perspective of the SN38 delivery, hydrophobic interior surface-mediated loading of SN38 with high payload is attractive because of its convenience for the nanocomplex preparation and its two choices of release mode—continuous release by slow diffusion and controlled burst release by NIR irradiation. The fluorescence microscopy images also supported the functional cellular uptake of SN38- and/ or FDz-loaded CHO-Hex-PVP-HANs into the NS3 replicon Huh7 cells, and NIR irradiation triggered burst release of loaded SN38/FDz. Compared to control, multitherapeutic treatment exhibited a significant decrease in cell viability and induced efficient cell death (Figure 5b).

CONCLUSION

In conclusion, PVP-coated hollow Au−Ag bimetallic nanoshells were prepared by galvanic replacement reaction and employed as a drug/gene codelivery vehicle through interior and exterior surface modifications. Apart from the exterior surface, the interior Au surface modifed with hydrophobic SAMs provided excellent local microenvironment to load hydrophobic drug

cargos with high payload while guaranteeing high dispersibility of the whole nanocomplex in aqueous solvent. In addition, SN38/FDz codelivery by using the PVP-HANs with NIR-mediated chemo-thermo gene multitherapeutic approach demonstrated advantages of not only the enhanced cargo payload of both hydrophobic and hydrophilic drugs but also high therapeutic potential in the treatment of hepatitis C in a cell-based model system. We expect that the present amphiphilic hollow nanoshells possessing hydrophobic interior and hydrophilic exterior structure will become one of the most promising options to choose for combinational treatment requiring gene therapy and chemotherapy due to high payload for both distinctive drugs and photothermal conversion-mediated controlled release of the loaded drugs in the near future.

METHODS

Materials. Hydrogen tetrachloroaurate(III) hydrate was purchased from Kojima Chemicals Co. (Sayama, Saitama, Japan). 3-(4,5-Dimethylthiazol-2-yl)-2,5-diphenyl tetrazolium bromide (MTT), anhydrous dimethyl sulfoxide, silver nitrate, ethylene glycol, hexanethiol, octanethiol, dodecanethiol, hexadecanethiol, glutaraldehyde, and poly(vinylpyrrolidone) (Mw 40 000) were purchased from

Sigma (St. Louis). Sodium hydroxide and sodium bicarbonate were purchased from Junsei (Tokyo, Japan). 10× phosphate-buffered saline (PBS), Dulbecco's modified eagle's medium (DMEM), and fetal bovine serum (FBS) were purchased from WelGENE (Seoul, Korea). LIVE/DEAD Viability/Cytotoxicity Assay Kit was purchased from Molecular Probes Invitrogen (Carlsbad, CA). G418 was purchased from A.G. Scientific, Inc. (San Diego, CA). SN38 (7-ethyl-10-hydroxycamptothecin) was purchased from TCI (Tokyo, Japan). All chemicals were used as received.

FAM-labeled DNAzyme amine (FAM-Dz-NH$_2$, FDz), which was designed against HCV NS3, was prepared as 5′-FAM-AAT GGG <u>GAG GCT AGC TAC AAC GA</u>G GCT TTG C-NH$_2$-3′ and purchased from Genotech (Seoul, Korea) (underlined letters: catalytic motif of DNAzyme).

Synthesis of PVP-AgNPs, PVP-HANs, CHO-PVP-HANs, and CHO-Hex-PVP-HANs. *Synthesis of 100 nm Sized PVP-AgNPs.* PVP (500 mg) was dissolved in 30 mL of ethylene glycol by ultrasonication and vigorous vortexing. The prepared PVP in ethylene glycol solution was heated to 170 °C followed by addition of 480 mg of silver nitrate which dissolved in 30 mL of ethylene glycol. The reaction mixture was boiled for 2 h with vigorous stirring and then cooled to room temperature by removing the oil bath. The obtained turbid yellow solution was rinsed with distilled water four times through centrifugation at 8000 rpm for 20 min each by Centrifuge 5810R (Eppendorf, Germany). Finally, PVP-AgNPs were redispersed in 200 mL of distilled water and stored in the dark.

Preparation of PVP-HANs by Galvanic Replacement Reaction. To 1 mL of the prepared 250 pM PVP-AgNPs, 100 μL of 1 mM hydrogen tetrachloroaurate(III) hydrate stock was added. After addition of Au(III) solution, the mixed solution was vigorously inverted several times and incubated for 10 min with shaking at room temperature. When the color change finished, the mixture was rinsed with distilled water four times using centrifugation at 8000 rpm for 20 min each. The final product was characterized by UV−vis spectrophotometry and stored at room temperature.

Preparation of CHO-PVP-HANs by Claisen-Schmidt Reaction. To 1 mL of the prepared 250 pM PVP-HANs, 100 μL of 1 mM glutaraldehyde stock solution in distilled water was added. Sodium bicarbonate was added to final concentration of 1 mM to adjust pH to 9. The mixed solution was incubated for 1 h with shaking at room temperature. After the reaction, the mixture was rinsed with distilled water four times using centrifugation at 8000 rpm for 20 min each. The final product was characterized by UV−vis spectrophotometry and stored at room temperature.

Preparation of CHO-Hex-PVP-HANs by Self-assembled Monolayer Formation. To 1 mL of the prepared 250 pM CHO-PVP-HANs, hexanethiol in ethanol was added to make the final concentration of 0.1 mM with a 1:9 ethanol/distilled water cosolvent system. The mixed solution was incubated for 2 h with shaking at room temperature. The mixture was rinsed with distilled water four times using centrifugation at 8000 rpm for 20 min each. The final product was characterized by UV−vis spectrophotometry and stored at room temperature.

Characterization of the Prepared PVP-AgNPs, PVP-HANs, CHO-PVP-HANs, and CHO-Hex-PVP-HANs. Energy-filtering transmission electron microscope LIBRA 120 (Carl Zeiss, Oberkochen, Germany) and high-resolution TEM and HAADF-STEM Tecnai F20 (FEI, Eindhoven, The Netherlands) were used to obtain images of nanoshells. UV−vis spectrometer S-3100 (Scinco, Seoul, Korea), Nanodrop2000 (Thermo Scientific, Waltham, MA), and SynergyMx (Biotek, Bedfordshire, U.K.) were used to obtain UV−vis absorption spectra. Fluorescence was measured by a spectrofluorometer FP-8300 (Jasco Inc., Easton, MD). Energy-dispersive spectroscopy was carried out by using EDAX (Ametek, NJ). NIR irradiation (808 nm) was performed by surgical lasers accessories OCLA (Soodogroup Co., Busan, Korea). Cell images were taken using an In-cell analyzer 2000 (GE Healthcare, Pittsburgh, PA, USA) and Ti inverted fluorescence microscope equipped with a 60× (1.4 numerical aperture) objective (Nikon Co., Chiyoda, Japan) with a CoolSNAP cf charge-coupled device (CCD) camera (Photometrics, Tucson, AZ) and BX51 M

optical microscope (Olympus Co., Tokyo, Japan) equipped with fluorescence light source and filters.

Characterization of Photothermal Effect. *Temperature Elevation Measurement.* To verify the temperature elevation by photothermal conversion, 1 mL of 200 pM PVP-AgNPs and PVP-HANs, CHO-Hex-PVP-HANs, and control distilled water were placed in quartz cuvette. The 808 nm NIR laser was irradiated to the sample solutions with intensity of 0.4 W/cm^2 for 2 min, and the temperature change was measured by a digital thermometer every 15 s.

Cell-Based Hyperthermia Measurement. To examine hyperthermia by photothermal conversion, PVP-HANs in 1× PBS was treated with NS3 replicon Huh7 cells in a six-well plate that were seeded with confluency of 50 000 cells per well with 1 day of pregrowth time. After 3 h of incubation in a humidified 5% CO$_2$ incubator at 37 °C, residual PVP-HANs were removed and washed with 1× PBS two times to get rid of remaining PVP-HANs, followed by replacement with serum-containing media. Next, the cells were irradiated with 808 nm NIR laser with intensity of 8 W/cm^2 for 5 min at ambient conditions, and incubated for an additional 2 h. Then media was removed and 200 μL of the combined live−dead cell-staining solution (2 μM calcein AM and 4 μM EthiD-1 in D-PBS) was added to each well and incubated for 15 min for staining. Fluorescent images of the cells were obtained using an inverted microscope equipped with fluorescence light source and filters.

Quantitative Measurement of Loading and Release of SN38 and FDz. *FDz Loading on CHO-Hex-PVP-HANs by Schiff Base Imine Linkage Formation.* Briefly, 10 μL of 1 mM FDz in distilled water stock solution was added to the prepared 1 mL of CHO-Hex-PVP-HANs (200 pM) and vigorously inverted for 20 s. To form the Schiff base primary imine bond, the pH of the mixture was set to 10 by addition of a small volume of sodium hydroxide solution. The reaction mixture was incubated for 3 h on a horizontally shaking plate at room temperature in the dark. The unbound substrate was removed by centrifugation at 8000 rpm for 20 min each and washed by using 25%, 50%, 75%, and 100% DMSO in distilled water sequentially. Finally, the obtained FDz-CHO-Hex-PVP-HANs were redispersed in 1 mL of DMSO and stored in the dark. The FDz conjugated PVP-HANs should be used as soon as possible to avoid dissociation of the loaded FDz. Calculation of the loaded SN38 was performed by using a UV−vis spectrophotometer with reported extinction coefficient ($\varepsilon_{SN38,380nm}$ = 25 500 L mol^{-1} cm^{-1}) based on Lambert−Beer's law.

SN38 Loading on FDz-CHO-Hex-PVP-HANs. To the prepared 1 mL of FDz-CHO-Hex-PVP-HANs (200 pM) in DMSO stock solution, 10 μL of 1 mM SN38 in DMSO was added and mixed well. To achieve the loading of SN38 to interior vacancy of nanoshells, the reaction mixture was incubated for 3 h on a horizontally shaking plate at room temperature in the dark. The unbound substrate was removed by centrifugation at 8000 rpm for 20 min each and washed by using 100%, 50%, 25%, and 10% DMSO in distilled water sequentially. Finally, FDz-CHO-Hex-PVP-HANs were redispersed in 1 mL of 1× PBS. Calculation of the loaded FDz was performed by using a UV−vis spectrophotometer and extinction coefficient of FDz ($\varepsilon_{FDz,260nm}$ = 8.86 × 10^5 L mol^{-1} cm^{-1}). Because of low UV−vis absorption of FAM, loading capacity of FDz was estimated by using UV−vis absorption of nucleobases of FDz (Figure S7).

SN38 and FDz Release Profile at Acidic (pH 5) and Neutral (pH 7.4) Conditions versus On/Off NIR Irradiation. To monitor the release of the loaded SN38 and FDz at pH 5 and pH 7.4 conditions, the concentrated SN38/FDz-CHO-Hex-PVP-HANs were dispersed in citrate buffer (pH 5.0) and phosphate-buffered saline (pH 7.4) solution at room temperature. At a designated time point, the solution of SN38/FDz-CHO-Hex-PVP-HANs was centrifuged at 14 000 rpm for 5 min by using Centrifuge 5418 (Eppendorf, Germany) to pull down the nanocomplex and the amount of the released SN38 and FDz was determined by measuring absorbance of supernatant at 380 and 260 nm, respectively. For NIR irradiation, 0.4 W/cm^2 NIR was repeatedly irradiated for 3 min, followed by 57 min intervals a total of 3 h. The measurement was carried out at the time points of 57, 60, 117, 120, 177, and 180 min.

Cellular Uptake. *Fluorescence Image of SN38- and/or FDz-Loaded CHO-Hex-PVP-HANs.* The SN38-CHO-Hex-PVP-HANs, FDz-CHO-Hex-PVP-HANs, and SN38/FDz-CHO-Hex-PVP-HANs in 1× PBS were used to treat the cultured NS3 replicon Huh7 cells with a density of 10 000 cells per well in a 96-well culture plate with 1 day of pregrowth time. After the treatment, the cells were incubated for 3 h in a humidified 5% CO_2 incubator at 37 °C. Residual nanoshells were then removed and washed with 1× PBS followed by replacement with fresh serum-containing media. The cells were irradiated with 808 nm NIR laser for controlled release of the loaded SN38/Dz and then incubated for another 1 h. Finally, the cells were observed by using an in-cell analyzer. Fluorescence of FDz was observed with a fluorescein isothiocyanate (FITC) (ex 495 nm)/FITC (em 521 nm) filter and SN38 was observed with a 4′,6-diamidino-2-phenylindole (ex 358 nm)/Cy3 (em 561 nm) filter.

Cell Viability Assay. *Cell Culture.* The NS3 hepatitis C virus RNA containing human hepatoma cell line Huh7 was grown in DMEM containing 4.5 g/L D-glucose, supplemented with 10% FBS (fetal bovine serum), 100 units/mL penicillin, 100 mg/mL streptomycin, and 500 μg/mL G418. The cells were grown in a humidified 5% CO_2 incubator at 37 °C.

MTT Assay for Cell Viability Measurement. MTT (3-(4,5-dimethylthiazol-2-yl)-2,5-diphenyl tetrazolium bromide) powder was dissolved in 1× PBS at 5 mg/mL concentrations and filtered through a 0.2 μm pore sized, sterilized syringe filter. The stock solution was stored at 4 °C. NS3 replicon Huh7 cells were seeded with a density of 10 000 cells per well of a 96-well culture plate with 100 μL of growth media (about 50−70% confluency). After cells were treated with free SN38, free FDz, SN38-CHO-Hex-PVP-HANs, FDz-CHO-Hex-PVP-HANs, and SN38/FDz-CHO-Hex-PVP-HANs with or without NIR irradiation, the cells were incubated for 24 h at 37 °C. Then the cells were rinsed with 1× PBS. Twenty microliter MTT stock solution was added to detect the metabolically active cells and the cells were incubated for 2−4 h until purple color developed. The media were discarded and 200 μL of DMSO was added to each well to make water-insoluble formazan salt solubilized. Then the optical densities of each well in the plates were measured at 560 nm. Mean and standard deviation of triplicates were calculated and plotted.

LIVE/DEAD Cell Staining. Cytotoxicity and hyperthermia effect of PVP-HANs and CHO-Hex-PVP-HANs were investigated by using the LIVE/DEAD Viability/Cytotoxicity Assay Kit. NS3 replicon Huh7 cells were seeded at 10 000 cells per well of a 96-well cell culture plate and 50 000 cells per well of a 6-well cell culture plate. The cells were incubated with dHAN3 at designated concentrations in 1× PBS for 4 h, then replaced with fresh media, and incubated for 20 h. Following incubation, 50 μL (96 well) or 200 μL (6 well) of the live−dead cell staining solution (2 μM calcein AM and 4 μM EthiD-1 in D-PBS) was added to each well and incubated for 30 min. Images were obtained using a microscope equipped with a fluorescence light source and filters.

ASSOCIATED CONTENT

Ⓢ Supporting Information

Analytical data and figures. The Supporting Information is available free of charge on the ACS Publications website at DOI: 10.1021/acsami.5b01903.

AUTHOR INFORMATION

Corresponding Author

*Phone: +82-2-880-4338. Fax: +82-2-889-1568. E-mail: dalheemin@snu.ac.kr.

Notes

The authors declare no competing financial interest.

ACKNOWLEDGMENTS

REFERENCES

(1) Prevo, B. G.; Esakoff, S. A. Scalable Route to Gold Nanoshells with Tunable Sizes and Response to Near-Infrared Pulsed-Laser Irradiation. *Small* **2008**, *4*, 1183−1195.

(2) Jackson, J. B.; Halas, N. J. Silver Nanoshells: Variations in Morphologies and Optical Properties. *J. Phys. Chem. B* **2001**, *105*, 2743−2746.

(3) Westcott, S. L.; Oldenburg, S. J.; Lee, T. R.; Halas, N. J. Construction of Simple Gold Nanoparticle Aggregates with Controlled Plasmon-Plasmon Interactions. *Chem. Phys. Lett.* **1999**, *300*, 651−655.

(4) Jang, H.; Kim, Y.-K.; Huh, H.; Min, D.-H. Facile Synthesis and Intraparticle Self-Catalytic Oxidation of Dextran-Coated Hollow Au-Ag Nanoshell and Its Application for Chemo-Thermotherapy. *ACS Nano* **2014**, *8*, 467−475.

(5) You, J.; Zhang, G.; Li, C. Exceptionally High Payload of Doxorubicin in Hollow Gold Nanospheres for Near-Infrared Light-Triggered Drug Release. *ACS Nano* **2010**, *4*, 1033−1041.

(6) El-Sayed, M. A. Some Interesting Properties of Metals Confined in Time and Nanometer Space of Different Shapes. *Acc. Chem. Res.* **2001**, *34*, 257−264.

(7) Sun, Y.; Mayer, B.; Xia, Y. Metal Nanostructures with Hollow Interiors. *Adv. Mater.* **2003**, *15*, 641−646.

(8) Auirre, C. M.; Moran, C. E.; Young, J. F.; Halas, N. J. Laser-Induced Reshaping of Metallodielectric Nanoshells Under Femtosecond and Nanosecond Plasmon Resonant Illumination. *J. Phys. Chem. B* **2004**, *108*, 7040−7045.

(9) Park, J.; Estrada, A.; Sharp, K.; Sang, K.; Schwartz, J. A.; Smith, D. K.; Coleman, C.; Payne, J. D.; Korgel, B. A.; Dunn, A. K.; Tunnell, J. W. Two-Photon-Induced Photoluminescence Imaging of Tumors Using Near-Infrared Excited Gold Nanoshells. *Opt. Express* **2008**, *16*, 1590−1599.

(10) Dewey, W. C. Arrhenius Relationships from the Molecule and Cell to the Clinic. *Int. J. Hyperthermia* **1994**, *10*, 457−483.

(11) Huang, X.; Jain, P. K.; El-Sayed, I. H.; El-Sayed, M. A. Determination of the Minimum Temperature Required for Selective Photothermal Destruction of Cancer Cells with the Use of Immunotargeted Gold Nanoparticles. *Photochem. Photobiol.* **2006**, *82*, 412−417.

(12) Loo, C.; Lowery, A.; Halas, N. J.; West, J. L.; Drezek, R. Immunotargeted Nanoshells for Integrated Cancer Imaging and Therapy. *Nano Lett.* **2005**, *5*, 709−711.

(13) Sershen, S. R.; Westcott, S. L.; Halas, N. J.; West, J. L. Temperature-Sensitive Polymer-Nanoshell Composites for Photothermally Modulated Drug Delivery. *J. Biomed. Mater. Res.* **2000**, *51*, 293−298.

(14) West, J. L.; Halas, N. J. Applications of Nanotechnology to Biotechnology: Commentary. *Curr. Opin. Biotechnol.* **2000**, *11*, 215−217.

(15) Boyer, D.; Tamarat, P.; Maali, A.; Lounis, B.; Orrit, M. Photothermal Imaging of Nanometer-Sized Metal Particles among Scatterers. *Science* **2002**, *297*, 1160−1163.

(16) Weissleder, R.; Ntziachristos, V. Shedding Light onto Live Molecular Targets. *Nat. Med.* **2003**, *9*, 123−128.

(17) Helmchen, F.; Denk, W. Deep Tissue Two-Photon Microscopy. *Nat. Methods* **2005**, *2*, 932−940.

(18) Weissleder, R. A Clearer Vision for *in vivo* Imaging. *Nat. Biotechnol.* **2001**, *19*, 316−317.

(19) Taguchi, T.; Isozaki, K.; Miki, K. Enhanced Catalytic Activity of Self-Assembled-Monolayer-Capped Gold Nanoparticles. *Adv. Mater.* **2012**, *48*, 6462−6467.

(20) Marshall, S. T.; O'Brien, M.; Oetter, B.; Corpuz, A.; Richards, R. M.; Schwartz, D. K.; Medlin, J. W. Controlled Selectivity for Palladium Catalysts Using Self-Assembled Monolayers. *Nat. Mater.* **2010**, *9*, 853−858.

(21) Schoenbaum, A.; Schwartz, D. K.; Medlin, J. W. Controlling the Surface Environment of Heterogeneous Catalysts Using Self-Assembled Monolayers. *Acc. Chem. Res.* **2014**, *47*, 1438−1445.

(22) Kim, Y.-K.; Ryoo, S.-R.; Kwack, S.-J.; Min, D.-H. Mass Spectrometry Assisted Lithography for the Patterning of Cell Adhesion Ligands on Self-Assembled Monolayers. *Angew. Chem., Int. Ed.* **2009**, *48*, 3507−3511.

(23) Aizenberg, J.; Black, A. J.; Whitesides, G. M. Control of Crystal Nucleation by Patterned Self-Assembled Monolayers. *Nature* **1999**, *398*, 495−498.

(24) Kato, M.; Mrksich, M. Rewiring Cell Adhesion. *J. Am. Chem. Soc.* **2004**, *126*, 6504−6505.

(25) Min, D.-H.; Tang, W.-J.; Mrksich, M. Chemical Screening by Mass Spectrometry to Identify Inhibitors of Anthrax Lethal Factor. *Nat. Biotechnol.* **2004**, *22*, 717−723.

(26) Montavon, T. J.; Li, J.; Cabrera-Pardo, J. R.; Mrksich, M.; Kozmin, S. A. Three-Component Reaction Discovery Enabled by Mass Spectrometry of Self-Assembled Monolayers. *Nat. Chem.* **2012**, *4*, 45−51.

(27) You, C.-C.; Miranda, O. R.; Gider, B.; Ghosh, P. S.; Kim, I.-B.; Erdogan, B.; Krovi, S. A.; Bunz, U. H. F.; Rotello, V. M. Detection and Identification of Proteins Using Nanoparticle-Fluorescent Polymer 'Chemical Nose' Sensors. *Nat. Nanotechnol.* **2007**, *2*, 318−323.

(28) Serefos, D. S.; Giljohann, D. A.; Hill, H. D.; Prigodich, A. E.; Mirkin, C. A. Nano-Flares: Probes for Transfection and mRNA Detection in Living Cells. *J. Am. Chem. Soc.* **2007**, *129*, 15477−15479.

(29) Chah, S.; Hammond, M. R.; Zare, R. N. Gold Nanoparticles as a Colorimetric Sensor for Protein Conformational Changes. *Chem. Biol.* **2005**, *12*, 323−328.

(30) Kim, C. K.; Ghosh, P.; Pagliuca, C.; Zhu, Z.-J.; Menichetti, S.; Rotello, V. M. Entrapment of Hydrophobic Drugs in Nanoparticle Monolayers with Efficient Release into Cancer Cells. *J. Am. Chem. Soc.* **2009**, *131*, 1360−1361.

(31) Pillai, P. P.; Huda, S.; Kowalczyk, B.; Grzybowski, B. A. Controlled pH Stability and Adjustable Cellular Uptake of Mixed-Charge Nanoparticles. *J. Am. Chem. Soc.* **2013**, *135*, 6329−6395.

(32) Mani, G.; Johnson, D. M.; Marton, D.; Feldman, M. D.; Patel, D.; Ayon, A. A.; Agrawal, C. M. Drug Delivery from Gold and Titanium Surfaces Using Self-Assembled Monolayers. *Biomaterials* **2008**, *34*, 4561−4573.

(33) Jang, H.; Min, D.-H. Spherically-Clustered Porous Au-Ag Alloy Nanoparticle Prepared by Partial Inhibition of Galvanic Replacement and Its Application for Efficient Multi-Modal Therapy. *ACS Nano* **2015**, *9*, 2696−2703.

(34) Schaefer, M.; Schmidt, F.; Folwaczny, C.; Lorenz, R.; Martin, G.; Schindlbeck, N.; Heldwein, W.; Soyka, M.; Grunze, H.; Koenig, A.; Loeschke, K. Adherence and Mental Side Effects During Hepatitis C Treatment with Interferon Alfa and Ribavirin in Psychiatric Risk Group. *Hepatology* **2003**, *37*, 443−451.

(35) Ramesh, M.; Ahlawat, P.; Srinivas, N. R. Irinotecan and Its Active Metabolite, SN-38: Review of Bioanalytical Methods and Recent Update from Clinical Pharmacology Perspectives. *Biomed. Chromatogr.* **2010**, *24*, 104−123.

(36) Santoro, S. W.; Joyce, G. F. A General Purpose RNA-Cleaving DNA Enzyme. *Proc. Natl. Acad. Sci. U.S.A.* **1997**, *94*, 4262−4266.

(37) Lohmann, V.; Korner, F.; Koch, J.; Herian, U.; Theilmann, L.; Bartenschlager, R. Replication of Subgenomic Hepatitis C Virus RNAs in a Hepatoma Cell Line. *Science* **1999**, *285*, 110−113.

(38) Wu, P.; Hwang, K.; Lan, T.; Lu, Y. A DNAzyme-Gold Nanoparticle Probe for Uranyl Ion in Living Cells. *J. Am. Chem. Soc.* **2013**, *135*, 5254−5257.

(39) Tack, F.; Noppe, M.; Van Dijck, A.; Dekeyzer, N.; Van Der Leede, B. J.; Bakker, A.; Wouters, W.; Janicot, M.; Brewster, M. E. Delivery of a DNAzyme Targeting c-myc to HT29 Colon Carcinoma Cells Using a Gold Nanoparticulate Approach. *Pharmazie* **2008**, *63*, 221−225.

(40) Ryoo, S.-R.; Jang, H.; Kim, K. S.; Lee, B.; Kim, K. B.; Kim, Y.-K.; Yeo, W.-S.; Lee, Y.; Kim, D.-E.; Min, D.-H. Functional Delivery of DNAzyme with Iron Oxide Nanoparticles for Hepatitis C Virus Gene Knockdown. *Biomaterials* **2012**, *33*, 2754−2761.

(41) Ebrahimnejad, P.; Dinarvand, R.; Sajadi, A.; Jaafari, M. R.; Nomani, A. R.; Azizi, E.; Rad-Malekshahi, M.; Atyabi, F. Preparation and *in vitro* Evaluation of Actively Targetable Nanoparticles for SN-38 Delivery Against HT-29 Cell Lines. *Nanomedicine* **2010**, *6*, 478−485.

(42) Gu, Q.; Xing, J. Z.; Huang, M.; He, C.; Chen, J. SN-38 Loaded Polymeric Micelles to Enhance Cancer Therapy. *Nanotechnology* **2012**, *23*, 205101.

(43) Morachis, J. M.; Mahmoud, E. A.; Almutairi, A. Physical and Chemical Strategies for Therapeutic Delivery by Using Polymeric Nanoparticles. *Pharmacol. Rev.* **2012**, *64*, 505−519.

(44) Im, S. H.; Lee, Y. T.; Wiley, B.; Xia, Y. Large-Scale Synthesis of Silver Nanocubes: the Role of HCl in Promoting Cube Perfection and Monodispersity. *Angew. Chem., Int. Ed.* **2005**, *44*, 2154−2157.

(45) Liu, Z.; Robinson, J. T.; Sun, X.; Dai, H. PEGylated Nanographene Oxide for Delivery of Water-Insoluble Cancer Drugs. *J. Am. Chem. Soc.* **2008**, *130*, 10876−10877.

(46) Rodriguez-Lorenzo, L.; de la Rica, R.; Alvarez-Puebla, A.; Liz-Marzan, L. M.; Stevens, M. M. Plasmonic Nanosensors with Inverse Sensitivity by Means of Enzyme-Guided Crystal Growth. *Nat. Mater.* **2012**, *11*, 604−607.

(47) Halperin, E. C.; Perez, C. A.; Brady, L. W.; Wazer, D. E.; Freeman, C.; Prosnitz, L. R. *Perez and Brady's Principles and Practice of Radiation Oncology*, 5th ed.; Lippincott Williams & Wilkins: Philadelphia, PA, 2007; p 637.